Conformational Investigation of a Cyclic Enterobacterial Common Antigen Employing NMR Spectroscopy and Molecular Dynamics Simulations†

Mikael Staaf,‡ Christer Höög,‡ Baltzar Stevensson,§ Arnold Maliniak,§ and Göran Widmalm*,‡

Department of Organic Chemistry and Division of Physical Chemistry, Arrhenius Laboratory, Stockholm University, S-106 91 Stockholm, Sweden

Received September 28, 2000; Revised Manuscript Received December 1, 2000

ABSTRACT: The three-dimensional structure of a cyclic enterobacterial common antigen (ECA) having four trisaccharide repeating units has been investigated by NMR spectroscopy and molecular dynamics simulations. Three different NMR parameters were determined: (a) ^{1}H,^{1}H cross-relaxation rates from NOE experiments were used for determination of proton−proton distances; (b) trans-glycosidic $^3J_{C,H}$ scalar coupling constants analyzed via a Karplus-type relationship provided information on torsion angles; and (c) ^{1}H,^{13}C one-bond dipolar couplings obtained in a dilute liquid-crystalline medium were interpreted in terms of the orientational order and molecular conformations. The molecular dynamics simulations of the dodecasaccharide were performed with explicit water and counterions, which are important factors that strongly influence molecular conformation. Subsequently, the results from computer simulation were used to generate a three-dimensional structure of the cyclic ECA which is consistent with the experimental NMR parameters.

Enterobacterial common antigen (ECA)[1] is a surface antigen shared by all members of the Enterobacteriaceae family. The only nonenterobacterial species containing ECA found so far is *Plesiomonas shigelloides* (Vibrionaceae) (*1*, *2*). Normally ECA is attached to the outer membrane of the bacteria via a glycophospholipid. In a few bacteria (R-mutants), the polysaccharide is linked to a lipid A core and becomes immunogenic (*2*, *3*). There have also been reports of a lipid-free cyclic form (*4*, *5*). The biological significance of ECA has not been clarified, but it is indicated that ECA is needed for the expression of the full pathogenic capacity of the bacteria (*2*). The repeating unit of ECA isolated from different sources has been investigated (*3*−*5*), revealing a trisaccharide structure, namely, →3)-α-D-Fuc*p*4NAc-(1→4)-*β*-D-Man*p*NAcA-(1→4)-α-D-Glc*p*NAc-(1→.

Previously, a conformational analysis of ECA was performed using ^{1}H,^{1}H NOE and molecular dynamics simulations in vacuo (*6*). In the present study, we investigate the conformation of a cyclic ECA having four repeating units. Experimental investigations comprise measurements of ^{1}H,^{1}H NOEs, ^{1}H,^{13}C trans-glycosidic scalar coupling constants ($^3J_{C,H}$), and ^{1}H,^{13}C residual dipolar couplings ($D_{C,H}$) in a weakly ordered phase. Molecular dynamics simulations with explicit water included were carried out and used together with the experimental results to generate a three-dimensional molecular structure of ECA in solution.

MATERIALS AND METHODS

Characterization and Sample Preparation. The ECA was purified from the polysaccharide fraction of a *Plesiomonas shigelloides* strain using gel permeation chromatography on a Superdex 30 column where the material eluted after the void volume. Structure elucidation by NMR spectroscopy and FABMS analysis (*m*/*z* 2.43 kDa corresponding to $[M+H]^+$) revealed a cyclic polysaccharide with four trisaccharide repeating units. The NMR chemical shifts of the anomeric resonances were δ_H 5.09 and δ_C 102.0 for α-D-Fuc4NAc, δ_H 4.83 and δ_C 99.9 for *β*-D-ManNAcA, and δ_H 4.95 and δ_C 94.3 for α-D-GlcNAc.

For NMR experiments in isotropic solution, ECA (8.0 mg) was dissolved in 600 μL of phosphate-buffered D_2O (10 mM, pD 7) to give a sugar concentration of 5.5 mM. The sample for measurement of residual dipolar couplings was prepared as follows: DMPC and DHPC were carefully weighed and dissolved in a phosphate-buffered D_2O (10 mM, pD 7) to give two stock solutions, each containing a total of 8.0% lipid (w/v). After sonication, the solutions were mixed to give a DMPC:DHPC molar ratio of 3:1, determined by integration of the peaks in the ^{31}P NMR spectrum. For better preservation of the lipid solution, CTAB was added to give a DMPC:CTAB molar ratio of 25:1 (*7*). Sample homogeneity of the dilute liquid crystal solutions was ensured by several cycles of cooling (0 °C), sonication, and heating (40 °C) and checked in the NMR spectrometer by measurement of the ^{2}H quadrupolar splitting. Sharp lines of equal height are obtained when the sample is homogeneous (*8*). Due to the high ordering of the system, the lipid concentration was diluted to 3.5% with the appropriate phosphate buffer. ECA

† This research was supported by the Swedish Natural Science Research Council and the Carl Trygger Foundation.

* Corresponding author. Tel: + 46 8 16 37 42; Fax: +46 8 15 49 08; E-mail: gw@organ.su.se.

‡ Department of Organic Chemistry.

§ Division of Physical Chemistry.

[1] Abbreviations: CTAB, *N*-cetyl-*N*,*N*,*N*-trimethylammonium bromide; DHPC, dihexanoylphosphatidylcholine; DMPC, dimyristoylphosphatidylcholine; ECA, enterobacterial common antigen; FABMS, fast atom bombardment mass spectrometry; ISPA, isolated spin-pair approximation.

10.1021/bi002282l CCC: $20.00
Published on Web 02/28/2001

(4.0 mg) was dissolved in 600 μL of the liquid-crystalline solution to give a sugar concentration of 2.7 mM.

NMR Spectroscopy. NMR experiments were performed on a Varian Inova 600 MHz spectrometer equipped with a 5 mm triple-resonance PFG probe, and all FIDs were processed using the VNMR software (Varian). Chemical shifts are reported in ppm relative to internal sodium 3-trimethylsilyl-[2,2,3,3-$^2H_4$]propanoate (δ_H 0.00) or external dioxane (δ_C 67.40). All experiments were performed at 25 °C except for the ordered phase of the liquid-crystalline solution (37 °C).

The ^{1}H,^{1}H NOESY experiments with mixing times of 50, 100, 200, and 400 ms were obtained with a sweep width of 4 kHz in both dimensions. Thirty-two transients of 2048 complex points were accumulated for 128 t_1-increments. The TPPI-States procedure was used for frequency discrimination in the indirect dimension (*9*). Prior to Fourier transformation, zero-filling to 4096×256 complex points was performed, and the data were treated with a shifted sine-bell window function in both dimensions. Integration of the cross-peaks was performed using the same integration limits at all mixing times. Normalized cross-relaxation integrals were obtained by division of the measured integrals by the auto-peak value at zero mixing time. This value was obtained by extrapolation of the exponential decaying curve fitting the integrated auto-peaks at each mixing time. NOE build-up curves were obtained from the normalized integrals at different mixing times, and the cross-relaxation rates were calculated by fitting to a second-order polynomial with mixing times ≤ 200 ms. The quality of the least-squares fits, expressed as the regression coefficient, was $R > 0.997$ in all cases.

The carbon−proton dipolar couplings ($D_{C,H}$) were measured in the ordered phase employing the ^{1}H,^{13}C-gHSQC technique. The experiment was performed with spectral widths of 3.8 kHz for ^{1}H and 10.6 kHz for ^{13}C using a modified pulse sequence where the peak separation was measured in the indirect dimension. In the ordered (37 °C) and isotropic (25 °C) phases, 120 and 64 transients, respectively, of 1024 complex points were accumulated for 1024 increments. The spectra were zero-filled 8 times prior to the spectral analysis.

Measurement of long-range ^{1}H,^{13}C coupling constants, $^3J_{C,H}$, was performed using a 1D proton-detected multiple-site selective ^{13}C excitation experiment according to Blechta et al. (*10*), with extensions of pulsed field gradients as proposed by Nishida et al. (*11*). The two gradients in the pulse sequence were set to 20 G cm^{-1} and durations of 2 and 0.5 ms. A half-Gaussian shaped pulse (*12*) of 50 ms duration was used for selective ^{13}C excitation and Hadamard shapes for two sites, which were generated using the program Pandora's Pulse Box (*13*). Spectral widths of 3.3 kHz were sampled with 16 384 complex points and 24 000 scans per selective excitation. The data were zero-filled 8 times and treated with a line broadening function prior to transformation. The coupling constants were extracted using the *J*-doubling procedure (*10*, *14*) with 8 or 16 delta functions in the frequency domain.

Computer Simulation. The molecular mechanics program CHARMM (*15*) (parallel version 25b2) with the force field PARM22 (Molecular Simulation Inc., San Diego, CA) was used for all simulations. This interaction model is similar to the carbohydrate force field developed by Ha et al. (*16*). The cyclic dodecasaccharide was built with the Quanta/CHARMm package (Molecular Simulation Inc.). In the initial structure, the glycosidic torsion angles ϕ (H1−C1−OX−CX) and ψ (C1−OX−CX−HX), where X is the substitution position in the aglyconic sugar residue, were in the conformational regions for syn states; i.e., the exo-anomeric effect governs the ϕ torsion, and the ψ torsion is close to eclipsed. It should be noted that in contrast to, e.g., a linear oligosaccharide ECA is constrained by the nature of its topology. The carboxylate groups of the ManNAcA residues were provided with sodium counterions to balance the charges. Initial conditions for the molecular dynamics simulations of ECA were prepared by placing the solute in a cubic water box with a side length of 49.66 Å containing 4096 TIP3P water molecules (*17*) and removing those that were closer than 2.5 Å to any solute atom. This procedure resulted in a system with the dodecasaccharide and 3894 water molecules which was energy-minimized using Steepest Descent (500 steps) followed by Adopted Basis Newton−Raphson until the root-mean-square gradient was less than 0.01 kcal mol^{-1} Å^{-1}. The system was heated from 100 to 300 K with 5 K increments for 8 ps followed by equilibration at 300 K for 100 ps continued by a production run for 500 ps. The weak-coupling method proposed by Berendsen et al. (*18*) was used for keeping the temperature constant during the simulation. Minimum image boundary conditions were used with a heuristic update frequency of the nonbonded list and a force shift cutoff (*19*) acting to 18 Å, using a dielectric constant of unity. The SHAKE algorithm (*20*), with a tolerance gradient of 10^{-4}, was used to restrain hydrogen−heavy atom bond stretch, and the time step was accordingly set to 2 fs. Two molecular dynamics simulations starting from the same energy-minimized conformation were performed using the above procedure but with different initial velocities. Simulations were performed on an IBM SP2 computer at the Center for Parallel Computers, KTH, Stockholm, using 32 nodes resulting in a CPU time of ∼29 h per 100 ps.

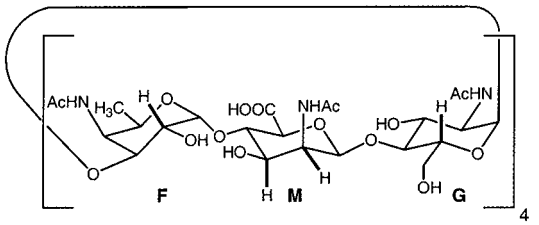

FIGURE 1: Schematic of the cyclic enterobacterial common antigen (ECA). Sugar residues are denoted as **F** (D-Fuc4NAc), **M** (D-ManNAcA), and **G** (D-GlcNAc). ^{1}H,^{13}C pairs for which dipolar couplings were determined are drawn in boldface type.

RESULTS AND DISCUSSION

The conformation of the cyclic ECA (Figure 1) in solution was investigated using NMR spectroscopy techniques and molecular dynamics (MD) simulations with explicit water. The proximity of protons at a glycosidic linkage is usually investigated by NOE spectroscopy. If a reference proton−proton pair with a known distance (r_{ref}) in the molecule can be identified, the isolated spin-pair approximation (ISPA) (*21*, *22*) makes it possible to extract unknown distances between protons *i* and *j* by comparing cross-relaxation rates

Table 1: Experimentally Determined NMR Parameters in the Sugar Residues of ECA

	F	M	G
$r_{H1,H3}$ (Å)[a]			2.66
$r_{H1,H4}$ (Å)	2.24	2.34	2.38
J_{ψ} (Hz)		5.4	5.4
$D_{C2,H2}$ (Hz)	11	−37	
$D_{C3,H3}$ (Hz)		55	
$D_{C5,H5}$ (Hz)			79

[a] Calculated using ISPA with a reference distance between H1 and H2 in **G** of 2.41 Å.

(σ_{ij}) according to

$$r_{ij} = r_{\mathrm{ref}}(\sigma_{\mathrm{ref}}/\sigma_{ij})^{1/6} \quad (1)$$

The cross-relaxation rates were obtained as the initial slopes in the NOE build-up curves from a series of NOESY experiments and used in eq 1 with the distance between H1 and H2 in residue **G** as a reference obtained from the MD simulation (vide infra). The resulting distances (Table 1) across the glycosidic linkages were both shorter and longer than the reference distance (2.41 Å). Also, intraresidual proton−proton distances in the other sugar residues were in good agreement (±0.13 Å) with those derived from the MD trajectory. The number of trans-glycosidic distance restraints is usually limited, which prevents an unambiguous interpretation of oligosaccharide conformation. Therefore, additional experimental parameters, such as *J* and *D* couplings, are necessary for 3D structure analysis.

Trans-glycosidic ^{1}H,^{13}C heteronuclear coupling constants, $^3J_{C,H}$, can be related to a glycosidic torsion angle (θ) via a Karplus-type relationship. In the present study, we have used the recently proposed equation given by (*23*):

$$^3J_{COCH} = 7.49\cos^2\theta - 0.96\cos\theta + 0.15 \quad (2)$$

Selected coupling constants are given in Table 1. The $^3J_{C,H}$-values related to the ϕ torsion angles were similar (∼4 Hz). The couplings corresponding to the ψ torsion angles, J_{ψ}, were 5.4 Hz (Table 1) for both the **M** and **G** residues. Due to spectral overlap, it was not possible to obtain the remaining J_{ψ} value for **F**. It should be noted that, due to the periodicity of a Karplus curve, up to four average torsion angles are consistent with a given value of $^3J_{C,H}$. This limitation in the interpretation is conveniently handled by resorting to MD simulations from which the averaged $^3J_{C,H}$ values can be calculated using eq 2.

The general expression for carbon−proton dipole−dipole couplings is given by (*24*):

$$D_{C,H} = -\frac{\mu_0}{4\pi}\frac{\gamma_C\gamma_H\hbar}{2\pi}\left\langle\frac{1}{2}(3\cos^2\zeta - 1)r_{CH}^{-3}\right\rangle \quad (3)$$

where r_{CH} is the spin−spin distance and ζ is the angle between the spin−spin vector and the magnetic field. All other symbols have their usual meanings. To derive the molecular conformation, i.e., the orientation of the C−H vector with respect to the molecular frame, eq 3 is written as

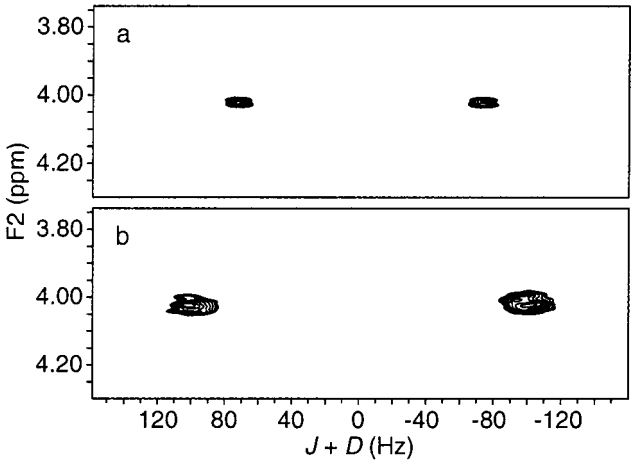

FIGURE 2: Part of the ^{1}H,^{13}C gHSQC NMR spectrum showing the cross-peak from H3/C3 in residue **M** at (a) 25 °C with splitting from spin−spin (*J*) coupling and at (b) 37 °C with a contribution from a dipole−dipole (*D*) coupling.

$$D_{C,H} = -\frac{\mu_0}{4\pi}\frac{\gamma_C\gamma_H\hbar}{2\pi r_{CH}^3}S_{zz}\left[\frac{1}{2}(3\cos^2\beta - 1)\right]\left[\frac{1}{2}(3\cos^2\eta - 1)\right] \quad (4)$$

where β is the angle between the spin−spin vector and the molecular symmetry axis, here defined by the normal of the molecular plane. The angle η defines the orientation of the phase director ($\eta = 90°$) with respect to the magnetic field, and S_{zz} is the order parameter. In eq 4, three important assumptions have been introduced: (i) the liquid-crystalline phase is uniaxial; (ii) the ECA molecule has uniaxial symmetry; and (iii) a single ordering matrix is used (indicating a rigid molecule). The presence of internal motion requires additional order parameters.

Residual dipolar couplings of the cyclic ECA were measured in a weakly ordered phase formed by bicelles. ^{1}H,^{13}C-HSQC spectra were acquired to obtain the $^1J_{C,H}$ couplings in the isotropic phase, whereas the splitting of the corresponding signals in the liquid-crystalline phase resulted from a sum of *J* and through-space dipolar couplings ($D_{C,H}$) (Figure 2). The residual dipolar couplings in the ordered phase, given in Table 1, were extracted by subtraction of the $^1J_{C,H}$ couplings determined in the isotropic phase. One geometrically independent dipolar coupling for each residue was obtained, except for residue **M** where two couplings with different vector orientations (see Figure 1) could be measured. We now have three types of independent NMR parameters that can be utilized in the analysis of the conformation of the cyclic ECA.

Computer simulations of the cyclic ECA were carried out with explicit water and sodium counterions. Two runs with different initial starting conditions were performed. The production parts of these simulations comprised 500 ps each, and are referred to as simulations I and II. In simulation I, a transition from ∼0° to ∼60° occurred for the ψ torsion angle of one of the **M** residues (Figure 3). As will be seen below, this torsion angle is of particular interest for the molecular conformation. Furthermore, transitions of this torsion angle may be of importance on a longer time scale

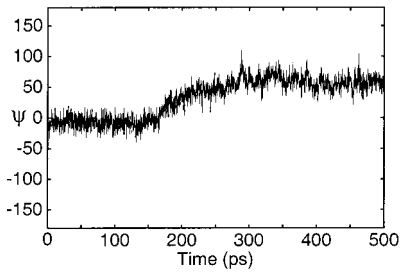

FIGURE 3: Molecular dynamics trajectory from simulation I showing the torsion angle ψ in one of the **M** residues. Note that a transition occurs between two conformational states for this torsion angle.

(vide infra). The conformations sampled for the torsion angles of all glycosidic linkages were essentially identical in the two simulations; i.e., the same conformational regions were populated by all torsions except for ψ in **M**, which exhibited two distinct conformational states. In the following, we focus the analysis on simulation II. The scatter plots of the 12 glycosidic linkages from simulation II are presented in Figure 4 and a summary of the torsion angles is given in Table 2. The scatter plots for residue **F** are quite similar in the different repeating units denoted A−D. The **G** residue reveals similarities pairwise for A and C in comparison to B and D, with ψ less negative in the latter case. The most significant shift of the torsion angles occurs in residue **M** where ϕ and ψ change ∼25° and 60°, respectively. Thus, the simulations indicate a structure with two conformational states possible for the three sugars in the repeating unit of the cyclic ECA.

In the following, the three relevant NMR parameters (proton−proton distances, coupling constants, and dipolar couplings) will be calculated using the trajectories as trial molecular structures. Subsequently, based on a comparison with the experimental data, a refined molecular structure will be generated. For each conformation in the MD trajectories, we calculated proton−proton distances as $r = \langle r^{-6} \rangle^{-1/6}$ and $\langle {}^3J_\psi \rangle$ according to eq 2. The distances and coupling constants derived from the trajectory generated in simulation II are collected in Table 2. The averages were calculated for each sugar residue in the dodecasaccharide and also averaged for each residue in the repeating unit. For the **F** residue, the trans-glycosidic distance from its anomeric proton to H4 of **M** is in much better agreement in repeats A and C compared to B and D. This trend is even more pronounced for the trans-glycosidic distance H1 in **M** to H4 in **G**. The anomeric proton in residue **G** exhibits two trans-glycosidic NOEs: to H3 and to H4 in **F**. In repeats A and C, the former distance is too long in the simulations whereas in repeats B and D it is too short. The latter distance shows the reverse pattern. In both cases, however, the differences

Table 2: Calculated Parameters of ECA from MD Simulation II

residue	ϕ (deg)	ψ (deg)	$r_{H1,H3}$ (Å)	$r_{H1,H4}$ (Å)	J_ψ (Hz)
A**F**	−39	−29		2.39 (−0.15)[a]	4.9
A**M**	60	0		2.44 (−0.10)	6.1 (−0.7)
A**G**	−62	−42	2.87 (−0.21)	2.28 (0.10)	3.5 (1.9)
B**F**	−62	−41		2.77 (−0.53)	3.7
B**M**	87	61		3.39 (−1.05)	1.9 (3.5)
B**G**	−51	−15	2.40 (0.26)	2.49 (−0.11)	5.4 (0.0)
C**F**	−31	−28		2.32 (−0.08)	4.9
C**M**	59	−7		2.37 (−0.03)	6.4 (−1.0)
C**G**	−61	−39	2.72 (−0.06)	2.31 (0.07)	3.9 (1.5)
D**F**	−61	−41		2.80 (−0.56)	3.6
D**M**	85	62		3.38 (−1.04)	1.6 (3.8)
D**G**	−51	−18	2.47 (0.19)	2.45 (−0.07)	5.1 (0.3)
<**F**>	−48	−35		2.51 (−0.27)	4.3
<**M**>	73	29		2.67 (−0.33)	4.0 (1.4)
<**G**>	−56	−28	2.54 (0.12)	2.37 (0.01)	4.5 (0.9)

[a] The difference (experimental − simulated) is given in parentheses.

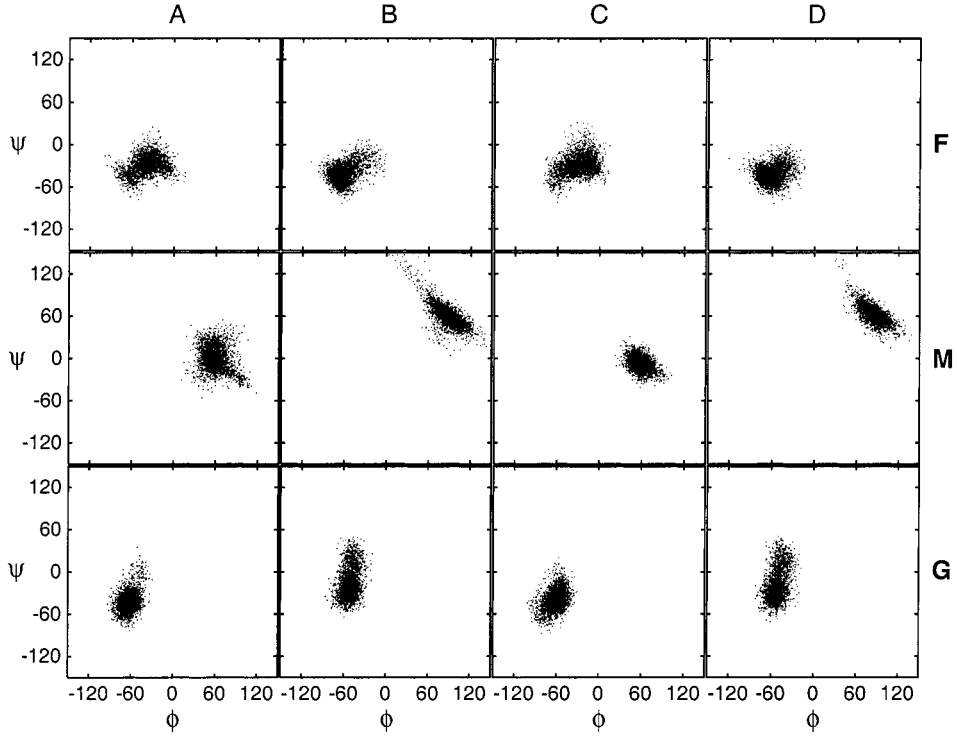

FIGURE 4: Scatter plots from MD simulation II showing the conformational regions sampled by the glycosidic linkages in ECA. Torsion angles ϕ and ψ run vertically and horizontally, respectively. Repeating units are denoted A−D (vertical) and sugar residues as **F**, **M**, and **G** (horizontal).

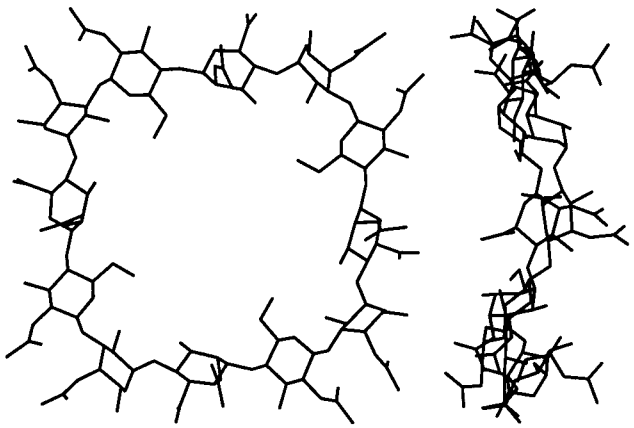

FIGURE 5: Three-dimensional structure of ECA generated from simulation and consistent with experimental data depicted as two orthogonal views.

are not large and the averaged structure <**G**> shows a reasonable agreement between distances derived from the computer simulation and experiments.

The analysis of the proton−proton distances indicates that the conformations of segments A and C in the trajectory are consistent with experimental results. It is therefore not surprising that similar trends are found for the ψ torsion angle in residue **M**. For residue **G**, however, the best agreement of ψ occurs for repeats **B** and **D**.

The dipolar couplings can be calculated from the MD trajectory using eq 4. Because there is no orientational order in the MD simulation, we need to determine a value of the order parameter S_{zz}. This can be done by fitting eq 4 to experimental dipolar couplings using averaged orientations of the C−H vectors, i.e., the β angles determined form the trajectory. These calculations indicate that the dipolar couplings are very sensitive to the molecular conformations, which in fact is in agreement with our previous investigations of a linear oligosaccharide (*25*). Using $S_{zz} = 4.6 \times 10^{-3}$, residue **F**, in repeats A and C, has the dipolar coupling $D_{C2,H2} \approx 30$ Hz whereas in B and D the same coupling is ≈ -20 Hz. Note, that the experimental value of this coupling is 11 Hz. A similar conformational behavior is also present for the **M** residue with $D_{C2,H2} \approx -20$ Hz in A and C and $D_{C2,H2} \approx 60$ Hz in B and D. The experimental value here is −37 Hz. The analysis of the dipolar couplings indicates that the molecular conformations corresponding to the A and C repeats exhibit best agreement with the experimental data.

We are now in a position to generate a three-dimensional structure of ECA. From the considerations of the NOEs, *J* couplings, and dipolar couplings presented above, it can be identified that the sequence B**G**-C**F**-C**M**- and likewise D**G**-A**F**-A**M**- may represent quite reasonable fragments in a molecular model of ECA in solution. To generate the cyclic dodecamer (Figure 5), we performed small modifications at the glycosidic torsion angles. The average torsion angles are described by the ϕ/ψ pairs being −32°(±10°)/7°(±10°), 30° (±10°)/27°(±2°), and −48°(±1°)/−38°(±1°) for **F**, **M**, and **G**, respectively. The J_ψ couplings derived from eq 2 using these torsion angles are 5.2 ± 0.2 and 4.1 ± 0.2 Hz for residues **M** and **G**, respectively. The trans-glycosidic proton−proton distances are 2.23 (±0.04) Å for H1**F**−H4**M**, 2.36 (±0.03) Å for H1**M**−H4**G**, 2.65 (±0.01) Å for H1**G**−H3**F**, and 2.37 (±0.04) Å for H1**G**−H4**F**. For these NMR parameters, very good agreement with experimental results (Table 1) is observed. The experimental dipolar couplings were then fitted to eq 4 using S_{zz} as an adjustable parameter. The result of the analysis is shown in Figure 6. We note that the structure is not perfectly symmetric and that the deviations of the vector orientations reflect the sensitivity of the technique to the conformation of the molecule.

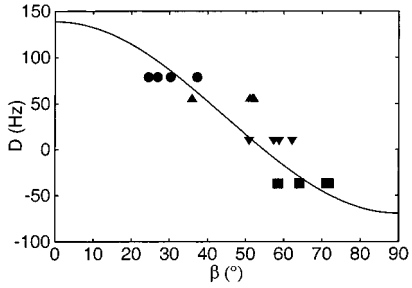

FIGURE 6: Residual dipolar couplings, $D_{C,H}$, calculated for each residue in the four repeating units of the cyclic ECA model (Figure 5) denoted by: (●) ($D_{C5,H5}$) in **G**; (▲) ($D_{C3,H3}$) in **M**; (▼) ($D_{C2,H2}$) in **F**; (■) ($D_{C2,H2}$) in **M**. The best fit curve using eq 4 with $S_{zz} = 7.1 \times 10^{-3}$ is included.

Cyclic glycans are products of several sources in Nature. The most well-known are probably cyclodextrins, i.e., cyclic glucans. NMR studies have been performed previously for different cyclic glucans including ^{13}C relaxation investigations of α- and γ-cyclodextrins (*26*) and the osmoregulated periplasmic glucan (OPG) of *Ralstonia solanacearum* (*27*). The former α-(1→4)-linked cyclic glucans with six or eight sugar residues are relatively rigid as deduced from their generalized order parameters close to unity. However, in the study of OPG which has 13 β-linked glucosyl residues, slow dynamics and conformational exchange was shown to be important. The discrepancy between experimental results and computer simulations for ECA may be due to limitations in the present force field, even though a significant restraint is present as a result of the cyclic structure. However, if the deviation is due to molecular motion via, e.g., pseudorotation along the cyclic structure, then the force field is probably of sufficient quality, but the simulation considerably too short. A pseudorotation could proceed via consecutive transitions of glycosidic torsion angles (cf. Figure 3) to produce additional molecular flexibility on a longer time scale. In the case of slow motions, one would need to investigate the system by NMR relaxation parameters such as exchange contributions to T_2 found for a ^{13}C-labeled OPG. However, for such studies to produce high quality data, ^{13}C enrichment of the sugar residues would be necessary.

We would also like to stress the importance of explicit water in the MD simulations. Initially, an MD simulation in vacuo with reduced charges of the carboxylate groups was performed. However, after a short simulation time, the three-dimensional structure of the cyclic dodecasaccharide collapsed, which resulted in a nonphysical structure. This behavior is completely analogous to an MD simulation of a mismatch DNA duplex previously performed (*28*). Both for ECA and for the DNA duplex, MD simulations with explicit water molecules alleviated the artificial structures generated in vacuo.

We have in this article presented an NMR investigation and computer simulation of ECA in solution. The aim was to determine the three-dimensional molecular structure. The

trajectory generated in the MD simulation was used to create an average trial molecular structure for analysis of the experimental results. Based on proton−proton distances, torsion angles, and residual dipolar couplings, we could identify sections of the molecule where the conformations were in good agreement with the experimental data. Subsequently, these fragments were used to generate a structure of the molecule which is consistent with the NMR parameters.

ACKNOWLEDGMENT

We thank Dr. D. Sandström for stimulating discussions.

REFERENCES

1. Kuhn, H.-M., Basu, S., and Mayer, H. (1987) *Eur. J. Biochem. 162*, 69−74.
2. Kuhn, H.-M., Meier-Dieter, U., and Mayer, H. (1988) *FEMS Microbiol. Rev. 54*, 195−222.
3. Lugowski, C., Romanowska, E., Kenne, L., and Lindberg, B. (1983) *Carbohydr. Res. 118*, 173−181.
4. Dell, A., Oates, J., Lugowski, C., Romanowska, E., Kenne, L., and Lindberg, B. (1984) *Carbohydr. Res. 133*, 95−104.
5. Vinogradov, E. V., Knirel, Y. A., Thomas-Oates, J. E., Shashkov, A. S., and L'vov, V. L. (1994) *Carbohydr. Res. 258*, 223−232.
6. Bruix, M., Jiménez-Barbero, J., and Philippe, C. (1995) *Carbohydr. Res. 273*, 157−170.
7. Losonczi, J. A., and Prestegard, J. H. (1998) *J. Biomol. NMR 12*, 447−451.
8. Ottiger, M., and Bax, A. (1998) *J. Biomol. NMR 12*, 361−372.
9. Marion, D., Ikura, M., Tschudin, R., and Bax, A. (1989) *J. Magn. Reson. 85*, 393−399.
10. Blechta, V., del Río-Portilla, F., and Freeman, R. (1994) *Magn. Reson. Chem. 32*, 134−137.
11. Nishida, T., Widmalm, G., and Sándor, P. (1996) *Magn. Reson. Chem. 34*, 377−382.
12. Friedrich, J., Davies, S., and Freeman, R. (1987) *J. Magn. Reson. 75*, 390−395.
13. Kupce, E., and Freeman, R. (1993) *J. Magn. Reson. 105*, 234−238.
14. McIntyre, L., and Freeman, R. (1992) *J. Magn. Reson. 96*, 425−431.
15. Brooks, B. R., Bruccoleri, R. E., Olafson, B. D., States, D. J., Swaminathan, S., and Karplus, M. (1983) *J. Comput. Chem. 4*, 187−217.
16. Ha, S. N., Giammona, A., Field, M., and Brady, J. W. (1988) *Carbohydr. Res. 180*, 207−221.
17. Jorgensen, W. L., Chandrasekhar, J., Madure, J. D., Impey, R. W., and Klein, M. L. J. (1983) *J. Chem. Phys. 79*, 926−935.
18. Berendsen, H. J. C., Postma, J. P. M., van Gunsteren, W. F., DiNola, A., and Haak, J. R. (1984) *J. Chem. Phys. 81*, 3684−3690.
19. Steinbach, P. J., and Brooks, B. R. (1994) *J. Comput. Chem. 15*, 667−683.
20. Ryckaert, J. P., Ciccotti, G., and Berendsen, H. J. C. (1977) *J. Comput. Phys. 23*, 327−341.
21. Keepers, J. W., and James, T. L. (1984) *J. Magn. Reson. 57*, 404−426.
22. Thomas, P. D., Basus, V. J., and James, T. L. (1991) *Proc. Natl. Acad. Sci. U.S.A. 88*, 1237−1241.
23. Cloran, F., Carmichael, I., and Serianni, A. S. (1999) *J. Am. Chem. Soc. 121*, 9843−9851.
24. Emsley, J. W., Ed. (1985) in *Nuclear Magnetic Resonance of Liquid Crystals*, Reidel, Dordrecht.
25. Landersjö, C., Höög, C., Maliniak, A., and Widmalm, G. (2000) *J. Phys. Chem. B 104*, 5618−5624.
26. Kowalewski, J., and Widmalm, G. (1994) *J. Phys. Chem. 98*, 28−34.
27. Lippens, G., Wieruszeski, J.-M., Horvath, D., Talaga, P., and Bohin, J.-P. (1998) *J. Am. Chem. Soc. 120*, 170−177.
28. Venable, R. M., Widmalm, G., Brooks, B. R., Egan, W., and Pastor, R. W. (1992) *Biopolymers 32*, 783−794.

BI002282L